1



# **Current Medical Imaging**

Content list available at: https://benthamscience.com/journals/cmir



# RESEARCH ARTICLE

# Predictive Factor of Tumor Aggressiveness in Patients with Extrahepatic Cholangiocarcinoma Based on Diffusion-weighted MRI

Xinqiao Huang<sup>1,#</sup>, Jian Shu<sup>1,\*</sup> and Jianmei Wang<sup>1</sup>

#### Abstract:

#### Background:

Extrahepatic cholangiocarcinoma (EHCC), an exceedingly malignant neoplasm, often eludes early detection, culminating in a dire prognosis. Accurate cancer staging systems and pathological differentiation are designed to guide adjuvant interventions and predict postoperative prognoses.

#### Objective:

This study sought to investigate the predictive capacity of DW-MRI in discerning T stages, lymph node metastasis, and pathological differentiation grades in patients with EHCC.

#### Methods:

Eighty-five patients were pathologically diagnosed with EHCC and underwent abdominal MRI within two weeks before surgery at our hospital from Aug 2011 to Aug 2021. Tumor axial maximum area (AMA) and apparent diffusion coefficient (ADC) values for diverse T stages, N stages, and differentiation grades were retrospectively analyzed.

#### Results

The Mann-Whitney U test displayed significantly higher lesion AMA values (P = 0.006) and lower tumor ADC values (P = 0.001) in the node-positive group (median ADC and AMA value:  $1.220 \times 10^{-3}$  mm²/s, 82.231 mm²) than in the node-negative group (median ADC and AMA value:  $1.316 \times 10^{-3}$  mm²/s, 51.174 mm²). A tumor ADC value< $1.249 \times 10^{-3}$  mm²/s from the receiver operating characteristic curve (AUC=0.725, P = 0.001) exhibited the capability to predict node-positive EHCC with a sensitivity of 64.29%, and specificity of 73.68%. Furthermore, a progressive decrease in the degree of EHCC differentiation was associated with a reduction in the tumor ADC value (P = 0.000).

#### Conclusion:

The N stage and differentiation of EHCC can be evaluated non-invasively using diffusion-weighted MRI.

**Keywords:** Extrahepatic cholangiocarcinoma, Neoplasm staging, Lymph node metastasis, Pathological differentiation grade, Diffusion-weighted imaging, The apparent diffusion coefficient value.

Article History Received: April 12, 2023 Revised: October 6, 2023 Accepted: October 12, 2023

# 1. INTRODUCTION

Cholangiocarcinoma (CC), an exceedingly malignant neoplasm, often eludes early detection, culminating in a dire

prognosis [1]. Emerging from cholangiocytes, this neoplasm is an infrequent occurrence [2]. The majority of CCs, approximately 90% to 95%, manifest as extrahepatic forms, classified into perihilar and distal subtypes [3]. Currently, the prevailing therapeutic modality for extrahepatic cholangiocarcinoma (EHCC) is radical resection, sometimes augmented by adjuvant chemotherapy [3, 4]. This combined approach demonstrates promise in ameliorating locoregional

Department of Radiology, The Affiliated Hospital of Southwest Medical University, 25 Taiping Street, 646000, Luzhou, Sichuan, People's Republic of China

<sup>&</sup>lt;sup>2</sup>Department of Pathology, The Affiliated Hospital of Southwest Medical University, 25 Taiping Street, 646000, Luzhou, Sichuan, People's Republic of China

<sup>\*</sup> Address correspondence to this author at the Department of Radiology, The Affiliated Hospital of Southwest Medical University, 25 Taiping Street, 646000, Luzhou, Sichuan, People's Republic of China; Tel: +86-18980253083; Fax: 0830-3165738; E-mail: shujiannc@163.com

 $<sup>\#\</sup> This\ author\ equally\ contributed$ 

recurrence and bolstering the overall survival of patients with EHCC [5, 6].

Notwithstanding these advancements, the prognosis of EHCC remains poor, as indicated by a five-year survival rate of merely 38% (range 15-54%) [7 - 9]. At the same time, EHCC has a high recurrence rate. Early recurrence (≤2.5 years) accounts for 80.8% of all recurrences [10]. The most significant risk factors for long-term survival are cancer staging systems (including T stage, lymph node and distant metastasis), pathological differentiation grade, and tumor location [11]. Cancer staging systems are designed to guide adjuvant interventions and predict postoperative prognoses. Notably, cases of EHCC associated with biliary tract obstruction exhibit a more favorable prognosis owing to the timely emergence of clinical manifestations.

Magnetic resonance imaging (MRI) is a non-invasive, high-resolution, and non-radiation imaging method for patients with different diseases [12]. Of note is the utility of diffusionweighted imaging (DWI), an MRI sequence enabling noninvasive evaluation of tissue microarchitecture and functional integrity at the cellular and molecular levels [13 - 15]. DWI finds broad application across diverse pathological contexts. The tumor apparent diffusion coefficient (ADC) value derived from DWI holds predictive potential for T stage in breast cancer, rectal cancer, and cervical cancer [16 - 18]. The ADC values also correlate with tumor differentiation grades of pancreatic adenocarcinoma, glioma, and hepatocellular carcinoma [19 - 21]. Furthermore, tumor ADC values bear relevance to lymph node involvement in colon cancer and breast cancer, as well as primary penile tumors [22 - 24]. However, limited data exist on the applicability of noninvasive DW-MRI in forecasting these EHCC-specific risk factors [25, 26]. This study sought to investigate the predictive capacity of DW-MRI in discerning T stages, lymph node metastasis, and differentiation grades in patients with EHCC.

#### 2. MATERIALS AND METHODS

#### 2.1. Patient Population

This study adhered rigorously to the principles delineated in the Helsinki Declaration and garnered requisite approval from the Ethics Committee of our hospital (Approval number: w2019001). Within two weeks preceding surgical intervention at our institution, patients underwent abdominal MR examination. This study was conducted from Aug 2011 to Aug 2021. All patients underwent abdominal MR examination before operation, chemotherapy, or radiotherapy. The records included general clinical messages, surgery records, MRI characteristics and pathological findings. All records underwent meticulous deidentification to ensure patient confidentiality. Consequently, the retrospective analysis encompassing patients diagnosed with EHCC obviated the necessity for informed consent.

Stringent inclusion and exclusion criteria governed eligibility for participation. Specifically, inclusion criteria included tumors confined exclusively to the extrahepatic biliary duct, while patients presenting with concurrent biliary tract injuries, acute pancreatitis, chronic pancreatitis, or

duodenal neoplasms were excluded based on pertinent diagnostic assessments. Furthermore, the fidelity of MR images in clearly portraying the targeted entities was mandatory.

Table 1. T stage for PHCC and DCC

Stage	Description (PHCC)	Description (DCC)
TX	Primary tumor cannot be assessed	Primary tumor cannot be assessed
ТО	No evidence of a primary tumor	No evidence of a primary tumor
Tis	Carcinoma in situ	Carcinoma in situ
T1	Tumor confined to the bile duct, with extension up to the muscle layer or fibrous tissue	Tumor invades the bile duct wall. The depth of invasion is< 5 mm
Т2	T2a: Tumor invades beyond the wall of the bile duct to surrounding adipose tissue; T2b: Tumor invades adjacent hepatic parenchyma	Tumor invades the bile duct wall. The depth of invasion is between 5 mm and 12 mm.
Т3	Tumor invades unilateral branches of the portal vein or hepatic artery	Tumor invades the bile duct wall, the depth of invasion is>12 mm
T4	Tumor invades the main portal vein or its branches bilaterally, or the common hepatic artery; or the second-order biliary radicals bilaterally; or unilateral second-order biliary radicals with contralateral portal vein or hepatic artery involvement.	Tumor involves the celiac axis, the superior mesenteric artery, or the common hepatic artery

Abbreviations: PHCC, perihilar cholangiocarcinoma; DCC, distal cholangiocarcinoma.

# 2.2. Histopathologic Analysis

All patients underwent surgical resection and paraffinembedded specimens for histopathologic analysis. Hematoxylin-eosin staining of tissue specimens was carried out by an adept histopathologist with over a decade of experience. This evaluation was deliberately blinded to individual participant data to mitigate bias.

EHCC is dichotomized into perihilar cholangiocarcinoma (PHCC) and distal cholangiocarcinoma (DCC). PHCC originates from the confluence of the right and left hepatic bile ducts along with the apex of ductus choledochus, while DCC originates from the apex of ductus choledochus to the duodenum ampulla [3]. The T stage of EHCC was stratified into the following four categories based on the American Joint Commission on Cancer (AJCC, 8th Edition) [27]: PHCC—T1 or lower, T2 (T2a or T2b), T3, and T4 (Table 1); DCC-T1 or lower, T2, T3, and T4 (Table 1). The N stage of EHCC was categorized into N0 and N1 based on the AJCC [27]. In alignment with the World Health Organization (WHO) grading system, EHCC can be microscopically stratified into welldifferentiated (G1), moderately differentiated (G2), and poorly differentiated (G3) categories, reflective of tumor cell atypia [28, 29].

#### 2.3. MRI Scan

Image acquisition hinged on a 3.0-T superconducting MR equipment (Philips Achieva, Holland) equipped with a quasar dual-gradient setup and a 16.0-channel phased-array Torso

coil. Prior to imaging, patients were instructed to fast for 4–8 hours while limited water intake was permitted. They were coached to maintain breath control and suspension during supine imaging.

The imaging procedure consisted of a scout acquisition. A reference scan for sensitivity encoding (SENSE) reconstruction showed in subsequent acquisitions, an axial breath-holding dual fast field echo (dual-FFE) T1-weighted imaging (T1WI), an axial breath-holding T1 High-Resolution Isotropic Volume Examination (THRIVE), a coronal turbo spin echo (TSE) T2-weighted imaging (T2WI), an axial Spectral Attenuated Inversion Recovery (SPAIR), an axial single-shot DWI with echo-planar imaging (EPI), a magnetic resonance cholangiopancreatography (MRCP), and a four-phase dynamic contrast enhanced-THRIVE.

The acquisition parameters for DWI were as follows: the TR was set to the shortest time, the TE was 70 ms. The flip angle was 90°. The echo train length (ETL) was 56, and the diffusion sensitivity coefficient (b) value was set to 0 and 800 s/mm² [12, 25]. The number of signal averages (NSA) was 4, the field of view (FOV) was 375, and the matrix size was 128×256. The slice thickness and gap were 7mm and 1 mm, respectively. There were 24 slices. The turbo factor was 45, and the EPI Factor was also 45.

#### 2.4. Image Analysis

Post-processing management of images was accomplished through the Extended MR Workspace R2.6.3.1 (Philip Healthcare) with the FuncTool package. In a randomized order, two seasoned radiologists independently reviewed and assessed image sets. Both radiologists, equipped with over five years of work experience, remained unaware of individual patient particulars and clinical or pathological findings. Consistency in assessment protocol and criteria was observed. Final quantification was predicated on averaged data from the two radiologists. Any discrepancies in visual interpretation were harmonized through consensus.

Documentation included tumor ADC value from the ADC map, lesion signal intensity (SI), and axial maximum area (AMA) value from DWI. Rigorous selection of regions of interest (ROI) avoids necrosis areas, calcifications, vascular structures and image artifacts. The ROI for AMA in the DWI image Fig. (1A) was assumed to be an irregular form mirroring the lesion's configuration. For enhanced precision and artifact mitigation, the ROI for ADC value was first established in a magnified, artifact-free DWI image Fig. (1B). Subsequently, this ROI was transposed onto the ADC map Fig. (1C) to automatically generate the ADC value. Alignment of both

ROIs with the lesion's center and maximal coverage was maintained. Adjacent normal hepatic parenchyma served as the reference entity for qualitative analysis. The lesion SI was visually observed and classified into three grades: high-intensity signal, iso-intensity signal, and low-intensity signal.

#### 2.5. Statistical Analysis

All data were imported into a commercially available statistical software package (version 23.0, SPSS Inc., Chicago, IL, US) for statistical analysis. Inter-observer agreement for the lesion SI was evaluated using  $\kappa$  statistics, with  $\kappa$  scores of 0.41–0.60, 0.61–0.80, and more than 0.80 indicating moderate, good, and excellent agreement, respectively. The agreement for the AMA and ADC value between the two radiologists were analyzed by using the interclass correlation coefficient (ICC), with an ICC over 0.75 indicating excellent interrater agreement [12, 25, 29].

Presentation of quantitative data adhered to mean ± standard deviation (SD) for normally distributed data and median values for non-normally distributed data. Statistical analyses encompassed analysis of variance for normally distributed, homogenous variance data and the Kruskal-Wallis H Rank-Sum test for other scenarios. Pairwise comparisons employed the Mann-Whitney U test with exact probability calculations. The accuracy of diagnostic criteria for the AMA and ADC values was determined by computing the area under the curve (AUC) from relevant receiver operative characteristics (ROC) curves. Diagnostic performance was classified as low, moderate, and excellent, with AUC ranges 0.50-0.70, 0.71-0.90, and above 0.90, respectively [29]. The best cut-off value is selected according to the maximum Youden index. Youden index = sensitivity - (1 - specificity). Statistical significance was predicated on a two-tailed test vielding a P of less than 0.05.

#### 3. RESULTS

## 3.1. Clinical and Pathological Findings

During the 10-year period of this study, a total of 157 consecutive patients were meticulously scrutinized against the stringent inclusion and exclusion criteria. This process resulted in the identification of 85 suitable participants whose clinical and pathological data are displayed in Table 2.

#### 3.2.1. Consistency between Observers

The agreement between observers for lesion SI ( $\kappa$  score=0.85), AMA (ICC=0.89), and ADC values (ICC=0.90) were notably robust (Table 3).

Table 2. Clinical and pathological data of patients with EHCC.

-	N (%)	Mean ± SD (Years)	Min ~ Max (Years)		
Total	85	57.15 ± 17.14	29~84		
Gender	-	-	-		
Male	48 (56.47%)	$56.65 \pm 8.79$	39~73		
Female	37 (43.53%)	58.71 ± 11.75	29~84		
Location	-	-	-		

(Table 2) contd....

-	N (%)	Mean ± SD (Years)	Min ~ Max (Years)		
PHCC	39 (45.88%)	-	-		
DCC	46 (54.12%)	-	-		
T stage	-	-	-		
T1	10 (11.76%)	-	-		
T2	30 (35.29%)	-	-		
Т3	43 (50.59%)	-	-		
T4	2 (2.36%)	-	-		
N stage	-	-	-		
N0	57 (67.06%)	-	-		
N1	28 (32.94%)	-	-		
Differentiation grade	-	-	-		
G1	29 (34.12%)	-	-		
G2	41 (48.23%)	-	-		
G3	15 (17.65%)	-	-		

Abbreviations: EHCC, extrahepatic cholangiocarcinoma; N, sample size; SD, standard deviation; Min, minimum; Max, maximum; PHCC, perihilar cholangiocarcinoma; DCC, distal cholangiocarcinoma; T stage, tumor stage; N stage, lymph node stage.

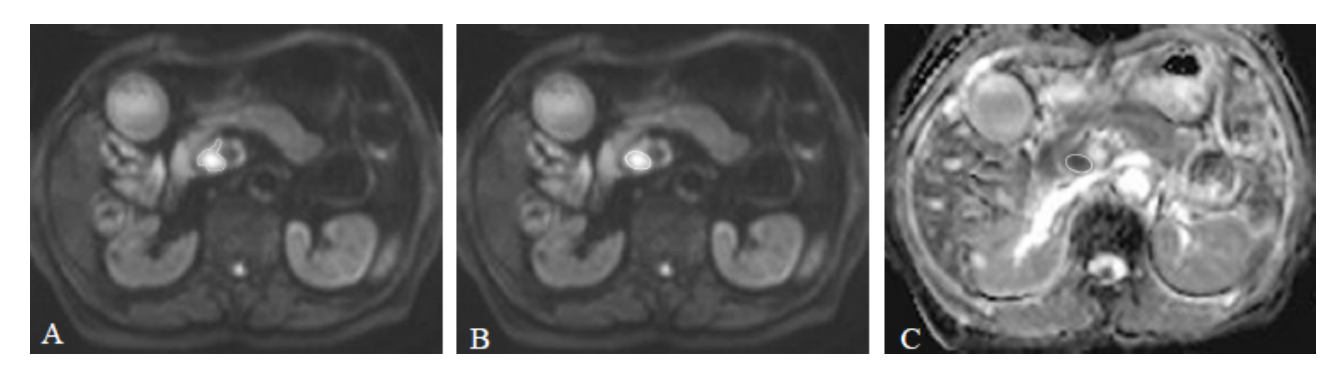


Fig. (1). The ROI for EHCC AMA value in the DWI image, and the ROI for ADC value in ADC map.

Description: Fig. (1A) shows the ROI (white irregular graph) for AMA value in the DWI image. Fig. (1B) displays the ROI (white round graph) for ADC value was first established in a magnified, artifact-free DWI image. Subsequently, this ROI was transposed onto the ADC map to automatically generate the ADC value. Alignment of both ROIs with the lesion's center and maximal coverage was maintained. Adjacent normal hepatic parenchyma served as the reference entity for qualitative analysis. The lesion SI were visually observed and classified into three grades: high-intensity signal, iso-intensity signal, and low-intensity signal.

Abbreviations: ROI, region of interest; EHCC, extrahepatic Cholangiocarcinoma; AMA, axial maximum area; DWI, diffusion-weighted imaging; ADC, apparent diffusion coefficient.

Table 3. The consistency between observers

Parameter	к (95%CI)	ICC (95%CI)		
The lesion SI	0.85 (0.76~0.94)	ī		
The lesion AMA	-	0.89 (0.78~0.97)		
The lesion ADC value	-	0.90 (0.86~0.95)		

Abbreviations: CI, confidence interval; SI, signal intensity; AMA, axial maximum area; ADC, apparent diffusion coefficient.

#### 3.2.2. Qualitative and Quantitative Findings in DWI

Out of the total EHCC cases, 82 exhibited different degrees of high-intensity signals in DWI images, rendering a diagnostic sensitivity of 96.47% (82/85). High-intensity lesions were detected in 100% (10/10) of patients in the T1 group, 97.50% (39/40) in the T2 group, 93.94% (31/33) in the T3 group and 100% (2/2) in the T4 group. Similarly, high-intensity lesions were found in 98.24% (56/57) of node-negative EHCC cases and 92.86% (26/28) of node-positive EHCC cases. Among patients with different degrees of pathological differentiation, high-intensity lesions were observed in 96.55% (28/29) of G1

cases, 95.12% (39/41) of G2 cases, and 100% (15/15) of G3 cases. There were no statistically significant differences in lesion SI across different T stages (P=0.754) and pathological differentiation grades (P=0.691) (Kruskal-Wallis H test) or N stages (P=0.219) (Mann–Whitney U test).

Analysis of lesion AMA values revealed deviations from normality in partial T stages (P=0.000 to 0.065) and N stages (P=0.000 and 0.352), as well as in all pathological differentiation grades (P=0.001, 0.000 and 0.014, respectively), as determined through the Shapiro Wilk test. Tumor median AMA values for diverse T stages, N stages, and pathological differentiation grades are displayed in Table 4. The Mann–Whitney U test showed significantly lower lesion AMA values in the node-negative group than in the node-positive group ( $x^2$ =7.660, P=0.006). Furthermore, the ROC curve for the AMA indicated a low diagnostic rate in node-positive EHCCs with an AUC value of 0.685 (P=0.006). Conversely, no significant differences in lesion AMA values were detected across different T stages ( $x^2$ =1.157, P=0.763) and tumor

differentiation grades ( $x^2 = 0.951$ , P = 0.621), as indicated by the Kruskal-Wallis H test.

## 3.2.3. Quantitative Findings in ADC Map

Lesions exhibited conspicuous high-intensity signals in DWI images while presenting low-intensity signals in the ADC map. Assessment of tumor ADC values demonstrated non-normal distribution across all T stages (P=0.000 to 0.031) and pathological differentiation grades (P=0.049, 0.000, and 0.013, respectively), as well as certain N stages (P=0.000 to 0.921), verified by the Shapiro Wilk test. The median ADC values for tumors within T stages, N stages, and degrees of pathological differentiation grades are displayed in Table 4. The tumor ADC values of EHCCs among groups at different T stages showed no statistically significant differences ( $x^2$  =1.554, P =0.670, Kruskal-Wallis H test). However, the tumor ADC values in the

node-negative group were statistically higher than those in the node-positive group ( $x^2=11.268$ , P=0.001, Mann–Whitney U test). The ROC curve for ADC values in predicting nodepositive EHCCs Fig. (2) yielded an AUC of 0.725 (P = 0.001), indicating moderate diagnostic accuracy with a cut-off value of  $1.249 \times 10^{-3} \text{ mm}^2/\text{s}$ . A tumor ADC value  $< 1.249 \times 10^{-3} \text{ mm}^2/\text{s}$  can forecast node-positive EHCCs with a sensitivity of 64.29% (18/28), specificity of 73.68% (42/59), the accuracy of 70.59% (60/85), the positive predictive value of 80.77% (42/52), and negative predictive value of 54.55% (18/33). Comparative analysis of lesion ADC values across various differentiation grades demonstrated statistically significant differences (x2=67.546, P = 0.000, Kruskal-Wallis H test). This was consistent across all pairwise comparisons (P = 0.000, Mann-Whitney U test). Notably, ADC values showed a statistically significant gradual increase in tandem with the progression of pathological differentiation grades in EHCCs.

# ROC Curve of Node-positive Group for ADC Value

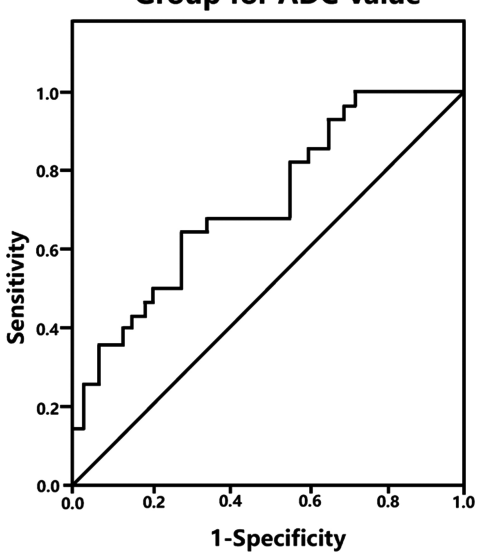


Fig. (2). The ROC curve for the ADC values predicting node-positive EHCC. Description: The AUC was 0.980 (P=0.000) with a cut-off value of  $1.249 \times 10^3$  mm<sup>2</sup>/s.

Abbreviations: ROC, receiver operating characteristic curve; ADC, apparent diffusion coefficient; EHCC, extrahepatic cholangiocarcinoma; AUC, area under the curve.

Table 4. Lesion AMA and ADC values for EHCCs in different T stages, N stages and pathological differentiation grades.

-	AMA value	Median and (mean ± SD) (mm²)	Min~ Max (mm²)	$x^2$	P	ADC value	Median and (mean ± SD) (×10 <sup>-3</sup> m <sup>2</sup> /s)	$ Min \sim Max  (\times 10^{-3} mm^2/s) $	$x^2$	P
T stage (n)	-	-	-	1.157	0.763	-	-	-	1.554	0.670
T1 (10)	-	55.774(72.012±33.027)	33.246~127.928	-	-	-	1.286(1.345±0.192)	1.176~1.708	-	-
T2 (40)	-	55.243(67.024±36.761)	29.773~154.833	-	-	-	1.287(1.313±0.191)	1.052~1.897	-	-
T3 (33)	-	73.448(76.452±40.972)	30.385~195.037	-	-	-	1.317(1.339±0.188)	0.925~1.951	-	-
T4 (2)	-	60.052(60.052±34.899)	35.374~84.729	-	-	-	1.220(1.220±0.189)	1.004~1.436	-	-
N stage (n)	-	-	-	7.660	0.006	-	-	-	11.268	0.001
N0 (57)	-	51.174(65.412±39.492)	29.773~195.037	-	-	-	1.316(1.375±0.196)	1.083~1.951	-	-
N1 (28)	-	82.231(82.699±31.251)	32.734~154.833	-	-	-	1.220(1.222±0.166)	0.925~1.475	-	-
Differentiation grade (n)	-	-	-	0.951	0.621	-	-	-	67.546	0.000

(Table 4) contd....

-	AMA value	Median and (mean ± SD) (mm²)	Min~ Max (mm²)	$x^2$	P	ADC value	Median and (mean ± SD) (×10 <sup>-3</sup> m <sup>2</sup> /s)	$ Min \sim Max  (\times 10^{-3} mm^2/s) $	$x^2$	P
T stage (n)	-	=	-	1.157	0.763	-	-	-	1.554	0.670
G1 (29)	-	55.414(69.264±41.297)	29.773~195.037	-	-	-	1.528(1.526±0.170)	1.317~1.951	-	-
G2 (41)	-	57.139(70.831±38.132)	30.295~154.833	-	-	-	1.256(1.260±0.054)	1.176~1.330	-	-
G3 (15)	-	87.729(75.424±30.499)	32.734~116.158	-	-	-	1.148(1.114±0.074)	0.925~1.183	-	-
Total (85)	-	59.294(71.107±37.689)	29.773~195.037	-	-	-	1.309(1.325±0.189)	0.925~1.951	-	-

Abbreviations: AMA, axial maximum area; ADC, apparent diffusion coefficient; EHCC, extrahepatic cholangiocarcinoma; T stage, tumor stage; N stage, lymph node stage; SD, standard deviation; Min, minimum; Max, maximum; n, sample size.

#### 4. DISCUSSION

The rapid development of MRI technology in medical research has ushered in remarkable improvements in EHCC diagnosis. Cutting-edge MRI techniques, encompassing comprehensive liver and bile duct evaluations, such as abdominal dynamic contrast-enhanced MRI, MRCP, and DWI, have firmly established themselves as the preferred diagnostic method. These methods not only facilitate EHCC diagnosis but also play a pivotal role in assessing resectability and monitoring recurrence in high-risk CC populations [30]. Particularly, DWI has emerged as an indispensable tool, swiftly and precisely revealing the spatial structure and tissue organization, as well as the dynamic water exchange properties influenced by pathological or physiological factors. The signal attenuation in DWI is closely linked to the micro-movement of water molecules and the perfusion of capillary microcirculation [14]. Due to its higher cell density than normal structures, EHCCs consistently exhibited SI in DWI images and reduced SI in ADC maps. To counteract the T2 shinethrough effect, we employed DWI images with different b values (low and high were 0 and 800 s/mm<sup>2</sup>, respectively). The primary objective of this study was to determine the utility of DWI in providing therapeutic strategies and prognostic assessments for clinical interventions.

Our findings revealed that tumor ADC values were significantly lower in EHCCs with lymph node metastases, particularly with a b value of 800 s/mm<sup>2</sup>. A tumor ADC value less than 1.249×10<sup>-3</sup> mm<sup>2</sup>/s exhibited the capability to predict node-positive EHCCs with a sensitivity of 64.29% (18/28), specificity of 73.68% (42/59), accuracy of 70.59% (60/85), positive predictive value of 80.77% (42/52), and negative predictive value of 54.55% (18/33). Furthermore, the variation in tumor ADC values correlated with pathological differentiation grades. Notably, G1 displayed higher values than G2, while G2 exhibited higher values than G3, with these differences demonstrating statistical significance. The augmented cell density, narrower extra-cellular gap, lower differentiation grades, and faster growth within EHCCs collectively contribute to restricted water molecule movement [31]. Meanwhile, a trend of ascended AMA values emerged in node-positive EHCCs, differentiating them from their nodenegative counterparts. However, AMA values exceeding 74.258 mm<sup>2</sup> fell short in predicting node-positive EHCCs, as indicated by a low diagnostic efficacy (AUC: 0.685, P =0.006). This observation could be attributed to the retrospective analysis of the study, the relatively low incidence of EHCCs, and the small sample size.

We also observed that MR-DWI could not distinguish

between different T stages of EHCCs based on ADC values. This could be attributed, in part, to the fact that numerous patients with advanced T4 stage and distant metastases did not undergo surgical intervention, thereby diminishing the living patient pool available for T4 tumor analysis and consequently attenuating the statistical significance of the differences observed. Similarly, differences in the AMA across EHCC T stages did not yield statistically significant differences, although the AMA varied based on pathological differentiation grades. Considering that the AMA represents the axial maximum area, its capacity to comprehensively represent the entire tumor might be limited, especially in cases involving adjacent anatomical regions.

However, it is imperative to acknowledge the limitations of this study. Despite the rigorous implementation of double-blind techniques, rigorous inclusion and exclusion criteria, and analysis of radiologists' decisions for consistency, the retrospective design introduces potential selection bias. Additionally, manual selection of the ROIs for tumor ADC values and AMA measurements introduces the potential for errors. Automated ROI measurements for ADC values and AMA could provide a more objective and preferable description of tumor features. Furthermore, the study's relatively limited patient cohort can be attributed to the low incidence of EHCC. The use of a minor matrix in DWI with EPI resulted in low spatial resolution and signal-to-noise ratio, leading to a low detection rate in DWI images.

Moreover, lesions < 5 mm in size are only visible in the presence of bile duct strictures (tumor in situ and infiltrative EHCC), and even when identified, measurement precision might be compromised. In some cases, the complexity of distinguishing between distal bile duct cancer and adjacent organ tumors exhibiting mutual invasion further underscored the study's limitations. The slender nature of the normal bile duct wall and the low spatial resolution in the ADC map precluded a comparison of ADC values between normal bile ducts and EHCC lesions. Lastly, the study lacked posttreatment patient follow-up, thus impeding the assessment of postoperative outcomes. In the future, larger-scale multicenter studies are indispensable to elucidate the correlations of the ADC value and AMA with treatment outcomes. We recommend monitoring patients' pre-treatment and posttreatment imaging. It is essential to emphasize that the role of DWI in EHCC remains exploratory, necessitating further investigations to solidify its clinical significance.

# CONCLUSION

In summary, the N stage and differentiation grade of EHCC can be assessed non-invasively using DW-MRI.

#### LIST OF ABBREVIATIONS

CC = Cholangiocarcinoma

DCC

EHCC = Extrahepatic cholangiocarcinoma

MRI = Magnetic resonance imaging

DWI = Diffusion-weighted imaging

ADC = Apparent diffusion coefficient

PHCC = Perihilar cholangiocarcinoma

**AJCC** = The American Joint Commission on Cancer

= Distal cholangiocarcinoma

**WHO** = The World Health Organization

G1 = Good-differentiation
G2 = Moderate-differentiation
G3 = Poor-differentiation
SENSE = Sensitivity encoding

dual-FFE = Dual fast field echoT1WI = T1-weighted imaging

THRIVE = T1WI high spatial resolution isotropic volume exam

TSE = Turbo spin echo
T2WI = T2-weighted imaging

**MRCP** = MR cholangiopancreatography

ETL = Echo train length

**b** value = The diffusion sensitivity coefficient value

NSA = Number of signal averages

**FOV** = Field of view

SI = Lesion signal intensity

AMA = Axial maximum area

ROI = Region of interest

ICC = The interclass correlation coefficient

SD = Standard deviation

ANOVA = The analysis of variance

AUC = The area under the curve

**ROC** = Receiver operative characteristics

# ETHICS APPROVAL AND CONSENT TO PARTICIPATE

Institutional Review Board approval was obtained from our hospital (Approval number: w2019001). All records underwent meticulous deidentification to ensure patient confidentiality. Consequently, the retrospective analysis encompassing patients diagnosed with EHCC obviated the necessity for informed consent.

#### **HUMAN AND ANIMAL RIGHTS**

No animals were used that are the basis of this study. All the human procedure were conducted according to the Declaration of Helsinki principles.

# CONSENT FOR PUBLICATION

Not applicable.

#### STANDARDS OF REPORTING

STROBE guidelines were followed.

#### AVAILABILITY OF DATA AND MATERIALS

The data supporting the findings of the article is available in the supplementary material.

#### **FUNDING**

None.

#### CONFLICT OF INTEREST

The authors have no conflicts of interest, financial or otherwise.

#### **ACKNOWLEDGEMENTS**

Declared none.

#### REFERENCES

- [1] Oliveira IS, Kilcoyne A, Everett JM, Mino-Kenudson M, Harisinghani MG, Ganesan K. Cholangiocarcinoma: Classification, diagnosis, staging, imaging features, and management. Abdom Radiol 2017; 42(6): 1637-49.
  [http://dx.doi.org/10.1007/s00261-017-1094-7] [PMID: 28271275]
- [2] Gad MM, Saad AM, Faisaluddin M, et al. Epidemiology of cholangiocarcinoma; united states incidence and mortality trends. Clin Res Hepatol Gastroenterol 2020; 44(6): 885-93. [http://dx.doi.org/10.1016/j.clinre.2020.03.024] [PMID: 32359831]
- [3] Tchelebi LT, Jethwa KR, Levy AT, et al. American radium society (ARS) appropriate use criteria (AUC) for extrahepatic cholangiocarcinoma. Am J Clin Oncol 2023; 46(2): 73-84. [http://dx.doi.org/10.1097/COC.0000000000000969] [PMID: 36534388]
- [4] Chaiteerakij R, Harmsen WS, Marrero CR, et al. A new clinically based staging system for perihilar cholangiocarcinoma. Am J Gastroenterol 2014; 109(12): 1881-90. [http://dx.doi.org/10.1038/ajg.2014.327] [PMID: 25384902]
- [5] Parente A, Kamarajah SK, Baia M, et al. Neoadjuvant chemotherapy for intrahepatic, perihilar, and distal cholangiocarcinoma: A national population-based comparative cohort study. J Gastrointest Surg 2023; 27(4): 741-9.
- [http://dx.doi.org/10.1007/s11605-023-05606-y] [PMID: 36749556]
   [6] Im JH, Choi GH, Lee WJ, et al. Adjuvant radiotherapy and chemotherapy offer a recurrence and survival benefit in patients with resected perihilar cholangiocarcinoma. J Cancer Res Clin Oncol 2021; 147(8): 2435-45.
  - [http://dx.doi.org/10.1007/s00432-021-03524-7] [PMID: 33471185] Juntermanns B, Kaiser GM, Reis H, *et al.* Long-term Survival after resection for perihilar cholangiocarcinoma: Impact of UICC staging
- and surgical procedure. Turk J Gastroenterol 2019; 30(5): 454-60. [http://dx.doi.org/10.5152/tjg.2019.18275] [PMID: 31061000]

  [8] Akashi K, Ebata T, Mizuno T, *et al.* Surgery for perihilar cholangiocarcinoma from a viewpoint of age: Is it beneficial to
- octogenarians in an aging society? Surgery 2018; 164(5): 1023-9.
  [http://dx.doi.org/10.1016/j.surg.2018.05.051] [PMID: 30082134]

  Zhou Y, Liu S, Wu L, Wan T. Survival after surgical resection of
- [9] Zhou Y, Liu S, Wu L, Wan T. Survival after surgical resection of distal cholangiocarcinoma: A systematic review and meta-analysis of prognostic factors. Asian J Surg 2017; 40(2): 129-38. [http://dx.doi.org/10.1016/j.asjsur.2015.07.002] [PMID: 26337377]
- [10] Zhang XF, Beal EW, Chakedis J, et al. Defining early recurrence of hilar cholangiocarcinoma after curative-intent surgery: A multiinstitutional study from the US extrahepatic biliary malignancy consortium. World J Surg 2018; 42(9): 2919-29. [http://dx.doi.org/10.1007/s00268-018-4530-0] [PMID: 29404753]
- [11] Mao Z, Guo X, Su D, Wang L, Zhang T, Bai L. Prognostic factors of cholangiocarcinoma after surgical resection: A retrospective study of 293 patients. Med Sci Monit 2015; 21: 2375-81. [http://dx.doi.org/10.12659/MSM.893586] [PMID: 26269932]
- [12] Shu J. Feasibility of magnetic resonance imaging-based radiomics features for preoperative prediction of extrahepatic

- cholangiocarcinoma stage. Eur J Cancer 2021; 155: 227-35.
- [13] Gluskin JS, Chegai F, Monti S, Squillaci E, Mannelli L. Hepatocellular Carcinoma and Diffusion-Weighted MRI: Detection and Evaluation of Treatment Response. J Cancer 2016; 7(11): 1565-70.
  - [http://dx.doi.org/10.7150/jca.14582] [PMID: 27471573]
- [14] Cadour F, Tradi F, Bartoli A, Duffaud F, Gaubert JY. Diffusion weighted imaging changes in extra-abdominal desmoid tumor after cryotherapy. Ann Med 2023; 55(1): 521-5. [http://dx.doi.org/10.1080/07853890.2023.2174589] [PMID: 367247581
- [15] Fujiwara M, Yoshida S, Takahara T, et al. Prostate and metastasis diffusion volume based on apparent diffusion coefficient as a prognostic factor in Hormone-naïve prostate Cancer. Clin Exp Metastasis 2023; 40(2): 187-95. [http://dx.doi.org/10.1007/s10585-023-10200-2] [PMID: 36914924]
- [16] Zhang M, Horvat JV, Bernard-Davila B, et al. Multiparametric MRI model with dynamic contrast□enhanced and diffusion□weighted imaging enables breast cancer diagnosis with high accuracy. J Magn Reson Imaging 2019; 49(3): 864-74.

  [http://dx.doi.org/10.1002/jmri.26285] [PMID: 30375702]
- [17] Zhou M, Gong T, Chen M, Wang Y. High-resolution integrated dynamic shimming diffusion-weighted imaging (DWI) in the assessment of rectal cancer. Eur Radiol 2023; 33(8): 5769-78. [http://dx.doi.org/10.1007/s00330-023-09494-3] [PMID: 36826497]
- [18] Liu L, Wang S, Yu T, et al. Value of diffusion-weighted imaging in preoperative evaluation and prediction of postoperative supplementary therapy for patients with cervical cancer. Ann Transl Med 2022; 10(2): 120.
  - [http://dx.doi.org/10.21037/atm-21-5319] [PMID: 35282103]
- [19] Zaboriene I, Zviniene K, Lukosevicius S, Ignatavicius P, Barauskas G. Dynamic perfusion computed tomography and apparent diffusion coefficient as potential markers for poorly differentiated pancreatic adenocarcinoma. Dig Surg 2021; 38(2): 128-35. [http://dx.doi.org/10.1159/000511973] [PMID: 33503636]
- [20] Wang Q, Zhang J, Xu X, Chen X, Xu B. Diagnostic performance of apparent diffusion coefficient parameters for glioma grading. J Neurooncol 2018; 139(1): 61-8. [http://dx.doi.org/10.1007/s11060-018-2841-5] [PMID: 29574566]
- [21] Xu YS, Liu HF, Xi DL, et al. Whole-lesion histogram analysis metrics of the apparent diffusion coefficient: A correlation study with histological grade of hepatocellular carcinoma. Abdom Radiol 2019; 44(9): 3089-98.

- [http://dx.doi.org/10.1007/s00261-019-02109-w] [PMID: 31256226]
- [22] Marija C, Kresimir D, Ognjen B, Iva P, Nenad K, Matija B. Estimation of colon cancer grade and metastatic lymph node involvement using DWI/ADC sequences. Acta Radiol 2022; 2841851221130008 [http://dx.doi.org/10.1177/02841851221130008] [PMID: 36197524]
- [23] De Cataldo C, Bruno F, Palumbo P, et al. Apparent diffusion coefficient magnetic resonance imaging (ADC-MRI) in the axillary breast cancer lymph node metastasis detection: A narrative review. Gland Surg 2020; 9(6): 2225-34. [http://dx.doi.org/10.21037/gs-20-546] [PMID: 33447575]
- [24] Barua SK, Kaman PK, Baruah SJ, et al. Role of Diffusion-weighted magnetic resonance imaging (DWMRI) in assessment of primary penile tumor characteristics and its correlations with inguinal lymph node metastasis: A prospective study. World J Oncol 2018; 9(5-6): 145-50.
  [http://dx.doi.org/10.14740/wjon1138w] [PMID: 30524639]
- [25] Cui XY, Chen HW, Cai S, et al. Diffusion-weighted MR imaging for detection of extrahepatic cholangiocarcinoma. Eur J Radiol 2012; 81(11): 2961-5. [http://dx.doi.org/10.1016/j.ejrad.2011.12.040] [PMID: 22285604]
- [26] Chen HW. Role of diffusion-weighted magnetic resonance imaging in the diagnosis of extrahepatic cholangiocarcinoma. World J Gastroenterol 2010; 16(25): 3196-201.
- [27] Amin MB, Edge SB, Greene FL. The American Joint Committee on Cancer Staging Manual. 8th ed. New York: Springer 2017. [http://dx.doi.org/10.1007/978-3-319-40618-3]
- [28] Griessenauer CJ, Miller JH, Agee BS, et al. Observer reliability of arteriovenous malformations grading scales using current imaging modalities. J Neurosurg 2014; 120(5): 1179-87. [http://dx.doi.org/10.3171/2014.2.JNS131262] [PMID: 24628617]
- [29] Huang XQ, Shu J, Luo L, Jin ML, Lu XF, Yang SG. Differentiation grade for extrahepatic bile duct adenocarcinoma: Assessed by diffusion-weighted imaging at 3.0-T MR. Eur J Radiol 2016; 85(11): 1980-6.
- [http://dx.doi.org/10.1016/j.ejrad.2016.09.004] [PMID: 27776649]
  [30] Jhaveri KS, Hosseini-Nik H. MRI of cholangiocarcinoma. J Magn Reson Imaging 2015; 42(5): 1165-79.
  [http://dx.doi.org/10.1002/jmri.24810] [PMID: 25447417]
- [31] Agnello F, Ronot M, Valla DC, Sinkus R, Van Beers BE, Vilgrain V. High-b-value diffusion-weighted MR imaging of benign hepatocellular lesions: Quantitative and qualitative analysis. Radiology 2012; 262(2): 511-9. [http://dx.doi.org/10.1148/radiol.11110922] [PMID: 22143926]

© 2024 The Author(s). Published by Bentham Science Publisher.



This is an open access article distributed under the terms of the Creative Commons Attribution 4.0 International Public License (CC-BY 4.0), a copy of which is available at: https://creativecommons.org/licenses/by/4.0/legalcode. This license permits unrestricted use, distribution, and reproduction in any medium, provided the original author and source are credited.